

# Spatial analysis of groundwater potential using weights-of-evidence and evidential belief function models and remote sensing

Naser Tahmassebpour<sup>1</sup> · Omid Rahmati<sup>1</sup> · Farhad Noormohamadi<sup>1</sup> · Saro Lee<sup>2</sup>

Received: 28 April 2015 / Accepted: 18 September 2015 / Published online: 22 December 2015  
© Saudi Society for Geosciences 2015

**Abstract** As demands for groundwater in the arid and semi-arid areas increase, delineation of groundwater potential zone becomes an increasingly valuable technique for implementing a successful groundwater potential analysis. The capability of using weights-of-evidence (WOE) and evidential belief function (EBF) models for groundwater potential mapping is tested and compared in the Ilam Plain, Iran. In the present study, multiple geo-environmental factors including lithology, land use, distance from river, soil texture, drainage density, altitude, curvature, topographic wetness index (TWI), slope percent, lineament density, and rainfall were used as inputs for both models. Subsequently, a well inventory map was produced using documentary sources of Iranian Water Resources Department (IWRD) and extensive field surveys. About 145 groundwater productivity data (with high potential yield values of  $\geq 11$  m<sup>3</sup>/h) were separated from well locations. Out of these, 101 (70 %) cases were randomly selected for groundwater potential modeling, and the remaining 44 (30 %) cases were applied for the validation purpose. In the next step, groundwater potential maps were produced using WOE and

EBF models in GIS environment. The receiver operating characteristic (ROC) curves for the produced maps were drawn and the areas under the curves (AUC) were determined. From the analysis, predictive performance of EBF model (AUC=83.7 %) was better than of WOE model (AUC=78.2 %). The results also show the capability of EBF model in managing uncertainty associated in groundwater potential mapping. Therefore, WOE and EBF models are shown to be an effective prediction models for groundwater potential mapping. The groundwater potential map can be helpful for planners in groundwater management and land use planning.

**Keywords** Groundwater potential modelling · GIS & RS · Weights-of-evidence · Evidential belief function · Iran

## Introduction

Water scarcity is the most important environmental challenge facing the arid and semi-arid regions. The demand on groundwater as one of the most valuable natural resources is increasing over the years, and the overexploitation of this water resource is threatening future generations (Todd and Mays 2005; Rekha and Thomas 2007). Therefore, proper assessment and planning of groundwater resource are key elements in the sustainable development of arid and semi-arid regions. The groundwater occurrence at any place on the given plain is not an issue of accidental but a result of the interrelationships among several factors such as hydrology, physiography, lithology, geological structures, drainage pattern, climatic conditions, landuse, and soil properties (Banks and Robins 2002; Jha et al. 2007; Ganapuram et al. 2009; Magesh et al. 2012; Nampak et al. 2014; Rahmati et al. 2014b). Spatial prediction of groundwater potential using a standard method is important

✉ Omid Rahmati  
Orahmati68@gmail.com; Omid\_Rahmati@ut.ac.ir

Naser Tahmassebpour  
Tahmasebi\_n@ul.ac.ir

Farhad Noormohamadi  
Fnoormihanmadi@gmail.com

Saro Lee  
leesaro@kigam.re.kr

<sup>1</sup> Department of Watershed Management Engineering, College of Natural Resources and Agriculture, Lorestan University, Khorramabad, Iran

<sup>2</sup> Geological Research Division, Korea Institute of Geoscience and Mineral Resources (KIGAM), 124 Gwahang-no, Yuseong-gu, Daejeon 305-350, South Korea

for groundwater management, especially under data-scarce and arid areas.

In recent years, research on groundwater resources potentiality has got international spotlight (Awawdeh et al. 2013; Manap et al. 2014; Mogaji et al. 2014; Fenta et al. 2015). Groundwater potential can be assessed using a variety of investigation methods (Madrucci et al. 2008; Prasad et al. 2008; Dar et al. 2010; Gupta and Srivastava 2010; Elewa and Qaddah 2011; Nag et al. 2012; Nag and Ghosh 2013; Nag and Saha 2014; Adji and Sejati 2014). The traditional methods of groundwater exploration through drilling, hydro-geological, geological, and geophysical techniques are extremely costly, and time-consuming (Todd and Mays 1980; Singh and Prakash 2002; Bevan et al. 2005; Israil et al. 2006; Jha et al. 2010). More recently, numerous studies have applied index-based models such as frequency ratio (FR) (Oh et al. 2011; Davoodi Moghaddam et al. 2015; Manap et al. 2014), certainty factor (Razandi et al. 2015), weights-of-evidence (WOE) (Corsini et al. 2009; Lee et al. 2012b), analytical hierarchy process (AHP) (Pradhan 2009; Manap et al. 2013; Kaliraj et al. 2014; Rahmati et al. 2014a; Shekhar and Pandey 2014; Fenta et al. 2015), information entropy (Chen et al. 2014), and logistic regression (LR) (Ozdemir 2011; Pourtaghi and Pourghasemi 2014) for assessing groundwater potentiality. Many researchers have also used soft computing techniques such as decision tree (DT) (Chenini and Mammou 2010), fuzzy logic (Shahid et al. 2002; Ghayoumian et al. 2007), boosted regression tree (BRT) (Naghibi and Pourghasemi 2015), Random forest (RF) (Rahmati et al. 2016), and artificial neural networks (ANN) (Corsini et al. 2009; Lee et al. 2012c) for groundwater potential mapping.

In a recent paper, Nampak et al. (2014) applied GIS-based data-driven evidential belief function (EBF) and logistic regression (LR) models in spatial prediction of groundwater potentiality of Malaysia. Their result indicated that EBF and LR models can be successfully applied in groundwater potential mapping. The EBF, based on the Dempster–Shafer (DS) theory of belief, was successfully applied as an effective model for landslide susceptibility mapping (Park 2011; Althuwaynee et al. 2012, 2014; Mohammady et al. 2012; Tien Bui et al. 2012) and mineral potential mapping (Carranza 2009). The DS theory of belief makes the framework for the determination of EBFs, which are integrated using combination rule of Dempster (1968) as a bivariate statistical analysis method. Tangestani and Moore (2002) stated that EBF model has robust theoretical basis (i.e., DS theory) which can manage uncertainties in multiresources spatial data integration. The EBF is a renowned spatial predictive model, a flexible approach useful in formalizing and addressing the problems of inappropriate management of uncertainty (Lee et al. 2012a, c) that allows analysis on both systemic and stochastic uncertainty (Mogaji et al. 2014). In contrast, the prior mentioned data mining models (e.g., FR, WOE) are

capable of only handling stochastic uncertainty; hence, the systemic uncertainty is ignored.

The principal objective of this paper was to produce groundwater potential maps (GPM) and their comparison using the GIS-based WOE and EBF models in the Ilam Plain, Iran. The important difference between current research and the approaches described in the aforementioned publications is that WOE and EBF models are mostly applied in landslide mapping (Park 2011; Mohammady et al. 2012; Pourghasemi et al. 2013b; Althuwaynee et al. 2014) and it is relatively new in groundwater potential mapping. In addition, current research is the pioneer work in identify the groundwater potentiality in the study area.

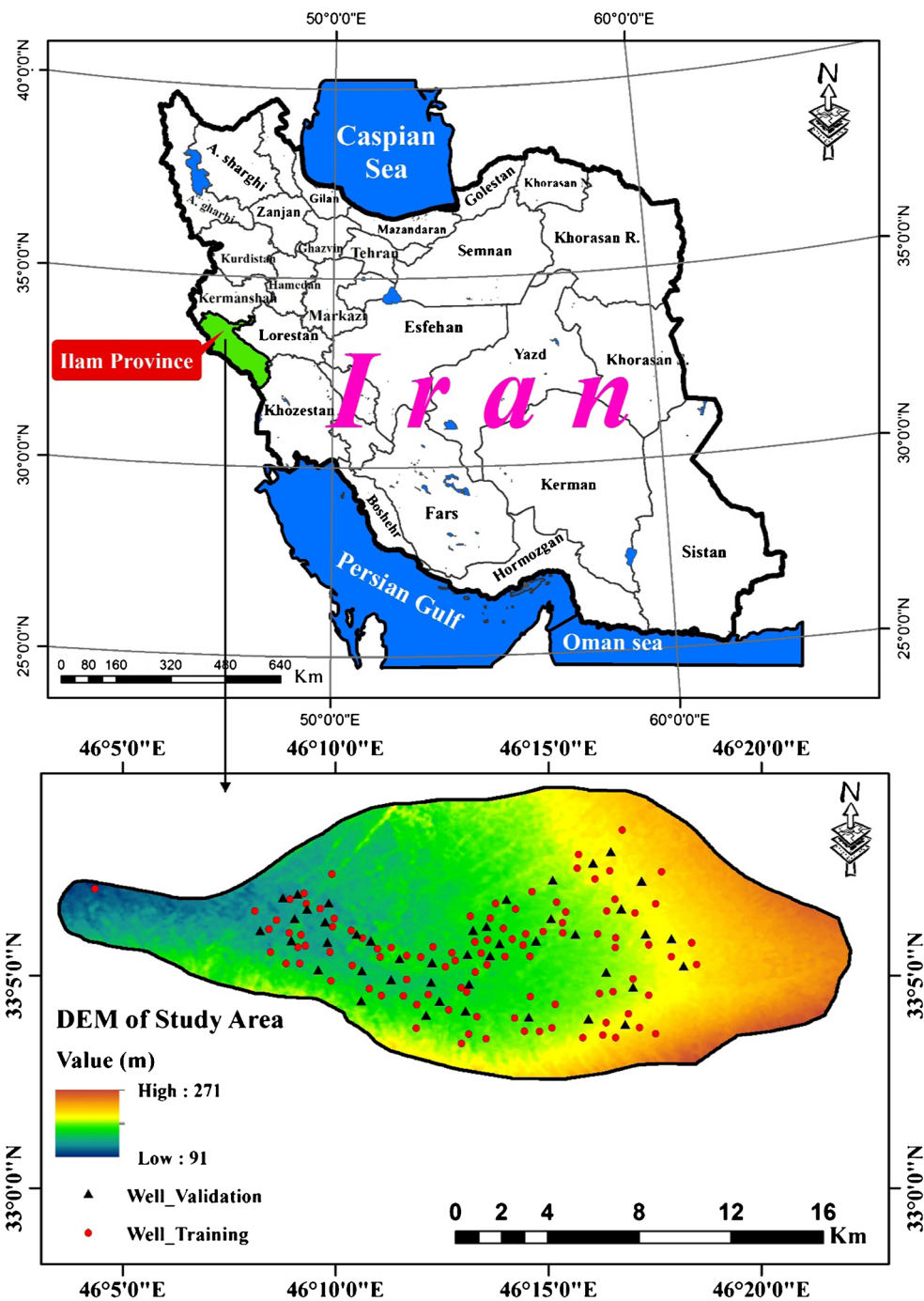
## Study area

The Ilam Plain is located in the northern part of Ilam Province, Iran, between latitudes 33° 2' to 33° 8' N, and longitudes 46° 03' to 46° 23' E (Fig. 1). It covers an area about 225.94 km<sup>2</sup> and its elevation ranges from 91 to 271 m above sea level, with an average of 105 m. The study area is considered to have a Mediterranean-type climate with an average annual rainfall of 320 mm (WRCI 2013). The study area receives approximately 85 % of its annual rainfall from December to April. In winter, temperature ranges from –8 to 10.5 °C, while in summer, it varies from 25 to 39 °C. From a geological viewpoint, the study area is located in Zagros structural zone of Iran. The Zagros is identified as a region of polyphase deformation, fracture systems, and the latest reflecting the collision of Arabia and Eurasia (Alavi 1994). The Ilam aquifer is considered as an unconfined in nature and is recharged across its entire surface by infiltrating rainfall and streams leaking into the subterranean system. According to geological survey of Iran (GSI 1997), the lithology of the study area is various (Table 1), and it is covered by conglomerate marly and sandy conglomerate with calcareous and clay matrix (Bk), conglomerate locally with sandstone (Plbk), and high level pediment fan and valley terrace deposits (Q<sub>n</sub>).

## Data

Data construction and collection of a spatial database of effective factors are essential part of any study (Chenini et al. 2010; Pourghasemi et al. 2013a). The groundwater information such as number of wells, yield, and depth were obtained from Iranian Department of Water Resources Management (IDWRM 2013), and extensive field surveys. Based on actual pumping test analysis of groundwater well, e.g., m<sup>3</sup>/h, the groundwater yield is specified. Because of limited accessibility of the groundwater data, indirect indicator of yield measurement was used in this investigation instead of hydraulic

**Fig. 1** Well locations with digital elevation model (DEM) map of the study area



constants of specific capacity as considered by Oh et al. (2011). The 145 groundwater productivity data with high

potential yield values of  $\geq 11 \text{ m}^3/\text{h}$  were selected from groundwater wells. The available groundwater wells data randomly

**Table 1** Lithology of the Ilam Plain, Iran

Code	Lithology	Formation	Geological age
Bk	Conglomerate marly and sandy conglomerate with calcareous and clay matrix	Bakhtyari	Pliocene
Pibk	Compacted conglomerate locally with sandstone	Bakhtyari	Pliocene
$Q_{ft}$	High level pediment fan and valley terrace deposits	–	Quaternary

were divided into two subsets. For preparing groundwater potential maps, 101 (70 %) cases of the groundwater wells were used, and the remaining 44 (30 %) were selected for validation. Figure 1 shows the groundwater well locations (training and validation datasets) in the study area.

Generally, the productivity and occurrence of groundwater in a given aquifer is affected by different effective parameters. The number of conditioning factors applied depends on the data accessibility in the study area. In current study, in order to assess groundwater potential zones, 11 groundwater conditioning factors were considered. These factors are lithology, landuse, distance from river, soil texture, drainage density, altitude, curvature, topographic wetness index (TWI), slope percent, lineament density, and rainfall. These conditioning factors provide a reliable database for an effective groundwater potential prediction of the study area in GIS framework (Fig. 2).

The lithology plays very important role in both the permeability and porosity of aquifer materials (Chowdhury et al. 2010; Adiat et al. 2012). The analogue geological map of the study area obtained from Iranian Department of Geological Survey (GSI 1997) with scale 1:100,000 was georeferenced and digitized in ArcGIS 10.2 software. Finally, the lithology map was classified into three groups as shown in Fig. 2a and Table 1.

In addition, landuse has an important role in the occurrence of groundwater and recharge process (Al Saud 2010; Fashae et al. 2014; Fenta et al. 2015). The landuse map for the study was extracted from Landsat ETM<sup>+</sup> image (May 27, 2013) through supervised classification of the false color composite (FCC) technique to produce the landuse category in ENVI 4.2 software. The landuse map of the area is shown in Fig. 2b. Four landuse types are present in the area and these are the agriculture, urban, range, and forest areas.

Rivers are the major sources of recharge, and then distance from rivers affect the groundwater potentiality in a given area. Euclidean distance tool in ArcGIS 10.2 software was used to generate distance from river categories, and then the prepared map was classified based on quantile classification scheme (Nampak et al. 2014) (Fig. 2c).

Soil texture is one of the most important factors in the surface runoff generation and infiltration process (Awawdeh et al. 2013; Mogaji et al. 2014). In this study, the soil texture is obtained from the digitized soil texture map of Ilam Plain, Iran. There are four classes of soil texture that exist in the study area: clay, sandy clay loam, clay loam, and sandy loam. The distribution of the soil texture can be seen in Fig. 2d.

The drainage system of an area is determined by the structure and type of the geological formation, the nature and attitude of the bedrock, and also by the slope degree (Adiat et al. 2012; Tehrani et al. 2013; Manap et al. 2014). From recharge process viewpoint, the characteristics of the drainage system govern the rate of surface water recharge into groundwater (Al

Saud 2010; Elmahdy and Mostafa Mohamed 2014). In order to determine the drainage density, the Line Density tool in ArcGIS 10.2 software was applied. Figure 2e shows the resulting map classified into four classes with the use of quantile classification method in the GIS environment (Nampak et al. 2014; Razandi et al. 2015).

A digital elevation model (DEM) with 30-m resolution was utilized (extracted from the 1:50,000-scale topographic map) to derive altitude layer. Altitude in the study area (91–271 m) were classified based on the quantile classification scheme (Razandi et al. 2015) which are <138, 138–162, 162–188, 188–217, and >271 m representing classes 1–5, respectively (Fig. 2f).

The useful geomorphological information can be obtained through the curvature analysis (Davoodi Moghaddam et al. 2015; Tehrani et al. 2014). In the case of curvature, negative curvature exhibits concave, zero curvature represents flat, and positive curvature depicts convex. Using ArcGIS 10.2, the curvature map of the area was produced and classified (Fig. 2g).

The TWI is a secondary topographic factor within the runoff model which has been widely utilized to express the impact of topography conditions on the location and size of saturated source zones of surface runoff generation (Davoodi Moghaddam et al. 2015). Also, the TWI of the study area has its own importance in affecting accumulation and movement of surface runoff over the land surface (Elmahdy and Mostafa Mohamed 2014). It is defined based on Eq. (1) (Moore et al. 1991):

$$TWI = \ln \left( \frac{Ac}{\tan \beta} \right) \quad (1)$$

where  $Ac$  is the cumulative upslope area draining through a point (per unit contour length) and  $\tan \beta$  is the slope angle at the point. In this study, TWI map was grouped into four classes using quantile classification method (Manap et al. 2014; Tehrani et al. 2014) (Fig. 2h).

The groundwater recharge processes (i.e., infiltration conditions) largely control by slope degree which always has an important role in groundwater potential mapping (Ettazarini and El Mahmoudi 2004; Ettazarini 2007; Al Saud 2010; Adiat et al. 2012). In the gentle slope area, the overland flow is slow allowing more time for rainwater to infiltrate and vice versa (i.e., infiltration rate is inversely related to slope angle) (Prasad et al. 2008). Therefore, the slope degree can be considered as surface indicator for assessing the groundwater potentiality. The slope percent map was produced from prepared DEM of the area using ArcGIS 10.2 software and was classified based on Natural Resources Management Agency of Iran (NRMAI 2005) (Fig. 2i).

Lineaments reflect rock structures and effect on the infiltration of surface runoff into subsurface (i.e., percolation

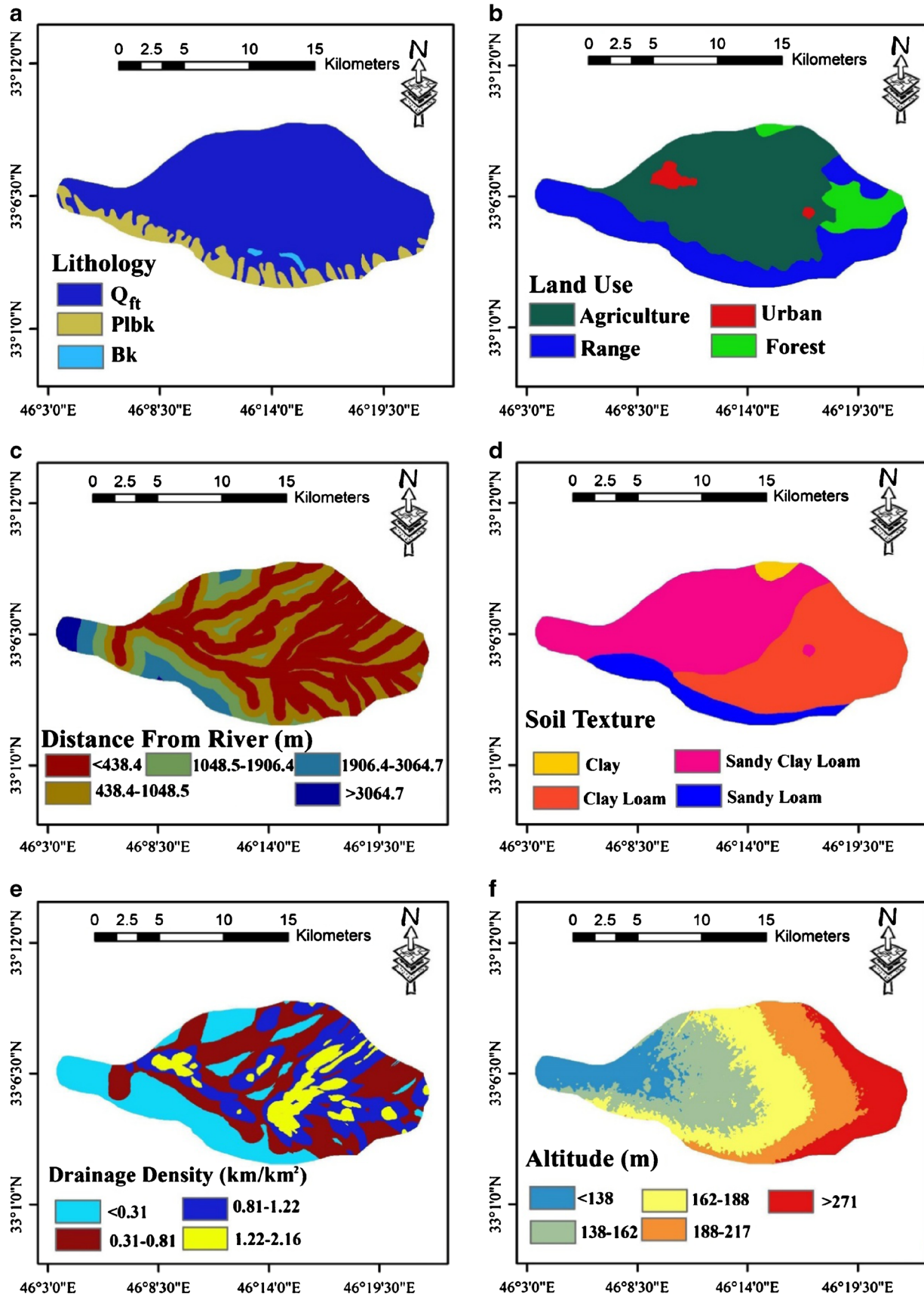


**Fig. 2** Input thematic layers. **a** Lithology. **b** Landuse. **c** Distance from river. **d** Soil texture. **e** Drainage density. **f** Altitude. **g** Curvature. **h** TWI. **i** Slope percent. **j** Lineament density. **k** Rainfall

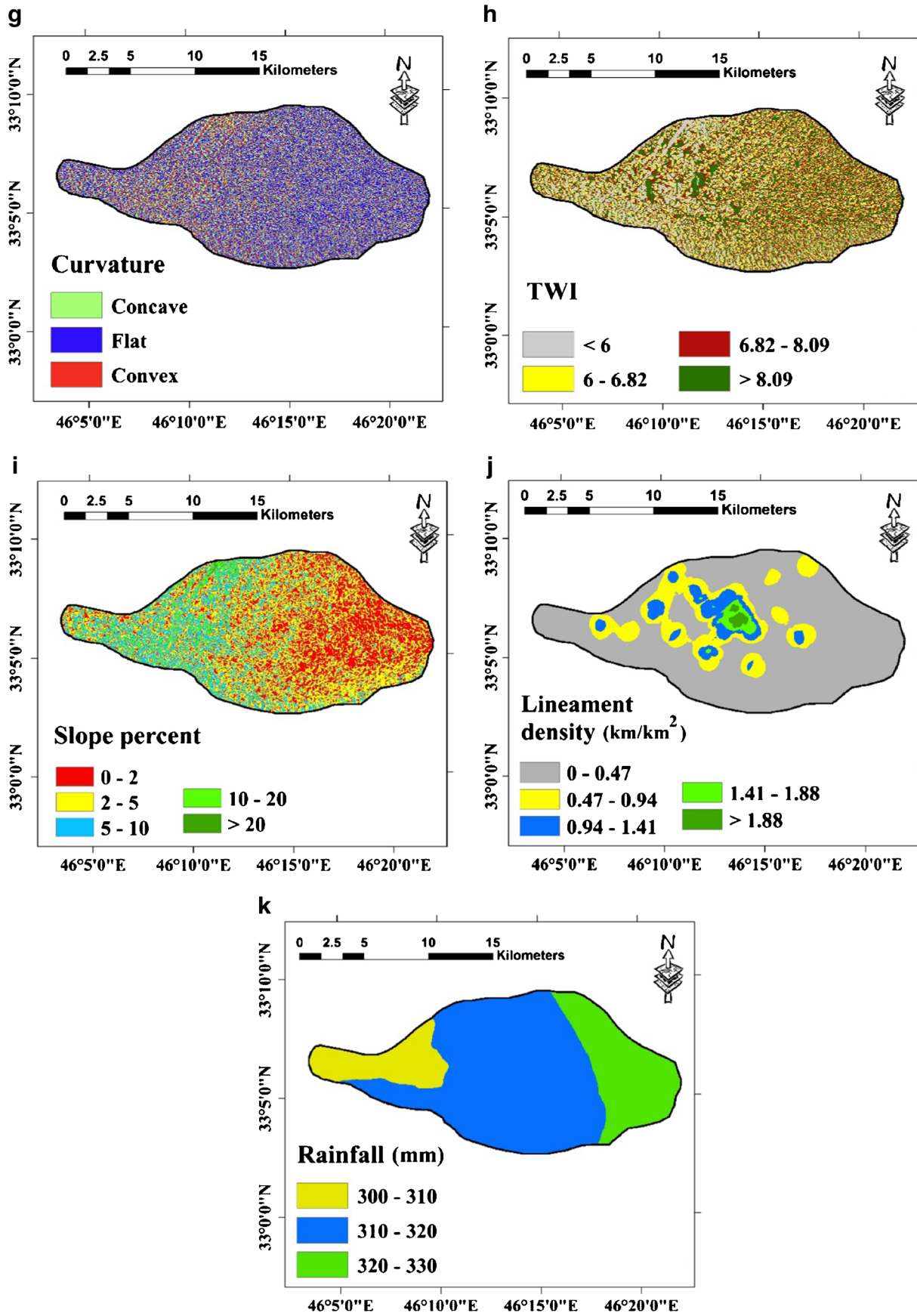


Fig. 2 (continued)

process) (Lee et al. 2012c; Fenta et al. 2015). To produce a lineaments map of the study area, edge enhancement and filtering (e.g., Sobel directional and high-pass directional) are done on the Landsat TM image. Subsequently, the lineament density was generated in ArcGIS by Line Density tool and classified into five classes based on equal interval classification method following Sener et al. (2005) and Hammouri et al. (2012) (Fig. 2j).

The rainfall availability was considered direct recharge source of groundwater (Adiat et al. 2012; Rahmati et al. 2014a). Mean annual rainfall data of five rain-gauge stations within the study area for a period of 25 years (i.e., 1990–2014) were obtained from the Meteorological Organization of Iran. The rainfall map is produced using inverse distance weight (IDW) interpolation technique and classified into three classes according to on Equal Interval classification scheme (Machiwal et al. 2011) (Fig. 2k).

### Methodology

The groundwater potential mapping contains of three phases: (1) geo-spatial database production (causal factors related to groundwater potential), (2) analysis of relationship between groundwater well locations (with high productivity) and groundwater causal factors, and (3) validation and comparison of prepared maps.

### Weights-of-evidence model

Weights-of-evidence (WOE) is a quantitative “data-driven” model based on Bayes rule used to predict probability of events. This model has been applied for groundwater spring potential mapping (Corsini et al. 2009; Ozdemir 2011; Lee et al. 2012a; Pourtaghi and Pourghasemi 2014). landslide susceptibility mapping (Pradhan et al. 2010; Pourghasemi et al. 2013b), debris flow prediction (Liu et al. 2006; Chang and Chien 2007), and flood susceptibility mapping (Tehrany et al. 2014). A detailed description of the mathematical of WOE model is expressed in Bonham-Carter (1991, 1994).

The method computes the weight for the presence or absence of each groundwater conditioning factor’s class ( $M$  or  $M^*$ ) based on the presence or absence of the well ( $N$  or  $N^*$ ) within the study area, as described in Bonham-Carter (1994) as follow:

$$W^+ = Ln \frac{P\left(\frac{M}{N}\right)}{P\left(\frac{M}{N^*}\right)} \tag{2}$$

$$W^- = Ln \frac{P\left(\frac{M^*}{N}\right)}{P\left(\frac{M^*}{N^*}\right)} \tag{3}$$

where  $P$  is probability,  $M$  is the presence of the groundwater conditioning factors,  $M^*$  is the absence of the groundwater conditioning factors,  $N$  is the presence of a well, and  $N^*$  is the absence of a well.

Positive weight ( $W^+$ ) and negative weight ( $W^-$ ) are the weights of evidence when a factor is present and absent, respectively (Corsini et al. 2009).

The difference between the  $W^+$  and  $W^-$  weights is noted as the weight contrast ( $C$ ) that in groundwater potential mapping reflects the spatial association between the conditioning factors and groundwater occurrences. A contrast value equal to zero reflects that the considered class of conditioning factors is not significant for the analysis, a negative contrast indicates a negative spatial correlation, and vice versa for a positive contrast (Corsini et al. 2009).

Moreover, the standard deviation  $S(C)$  of  $W$  can be calculated as follows (Eq. 4):

$$S(C) = \sqrt{S^2(W^+) + S^2(W^-)} \tag{4}$$

where  $S^2(W^+)$  and  $S^2(W^-)$  are the variance of the  $W^+$  and the variance of the  $W^-$ , respectively. The  $S^2(W^+)$  and  $S^2(W^-)$  can be determined as follows (Bonham-Carter 1994):

$$S^2(W^+) = \frac{1}{N\{F \cap E\}} + \frac{1}{F \cap \bar{E}} \tag{5}$$

$$S^2(W^-) = \frac{1}{\{\bar{F} \cap E\}} + \frac{1}{\{F \cap \bar{E}\}} \tag{6}$$

The studentized contrast (noted as  $\tau$ ) is a measure of confidence and can be determined using the following equation:

$$\tau = \left( \frac{C}{S(C)} \right) \tag{7}$$

In the application of WOE model, groundwater-related thematic maps were overlapped with the training well map. On the basis of these intersections,  $W^+$ ,  $W^-$ ,  $C$ ,  $S(C)$ , and  $\tau$  values were determined for each geo-environmental factor using Eqs. (4), (5), (6), and (7). After determination of  $\tau$  values, groundwater potential index (GWPI) was calculated for each pixel in the study area by the following expressions:

$$GWPI = \sum_{R=1}^{R=n} \tau \tag{8}$$

### Evidential belief function model

The evidential belief function (EBF) model is based on the Dempster–Shafer theory (DST) in generalization of Bayesian lower and upper probabilities (Dempster 1968; Shafer 1976).

The EBF model contains degree of belief (Bel), degree of disbelief (Dis), degree of uncertainty (Unc), and degree of plausibility (Pls) (Carranza and Hale 2003; Carranza et al. 2008; Althuwaynee et al. 2012). As characteristics of the EBF model, the values of Dis, Bel, and Unc each fall in the range [0, 1], and the sum of Dis, Bel, and Unc is 1 (Carranza et al. 2005; Lee et al. 2012a). Figure 3 illustrates the schematic relationships of Bel, Pls, Unc, and Dis.

In groundwater potential mapping based on the EBF model, a structure of discernment can be considered as follows (Mogaji et al. 2014; Nampak et al. 2014; Pourghasemi and Beheshtirad 2014):

$$m = 2^\Theta = \left\{ \phi, T_P, \overline{T}_P, \Theta \right\} \text{ With } \Theta = \left\{ T_P, \overline{T}_P \right\} \quad (9)$$

where

- $T_P$  Class pixels affected by groundwater well.
- $\overline{T}_P$  Class pixels not influenced by groundwater well
- $\phi$  Empty set

Based on Eq. (9), the belief function (Bel) can be calculated as (Park 2011):

$$\left[ \lambda(T_P)_{A_{ij}} \right] = \left[ \frac{N(W \cap A_{ij})}{N(W)} \right] / \left[ \frac{N(A_{ij} - N(W \cap A_{ij}))}{N(P) - N(W)} \right] \quad (10)$$

$$(\text{Bel}) = \left( \frac{\left[ \lambda(T_P)_{A_{ij}} \right]}{\sum \left[ \lambda(T_P)_{A_{ij}} \right]} \right) \quad (11)$$

where  $N(W \cap A_{ij})$  is the density of groundwater well pixels that occurred in  $A_{ij}$ ,  $N(W)$  is the total density of whole groundwater well that have presented in the study area,  $N(A_{ij})$  is the density of pixels in  $A_{ij}$ , and  $N(P)$  is the density of pixels in the whole study area  $P$ .

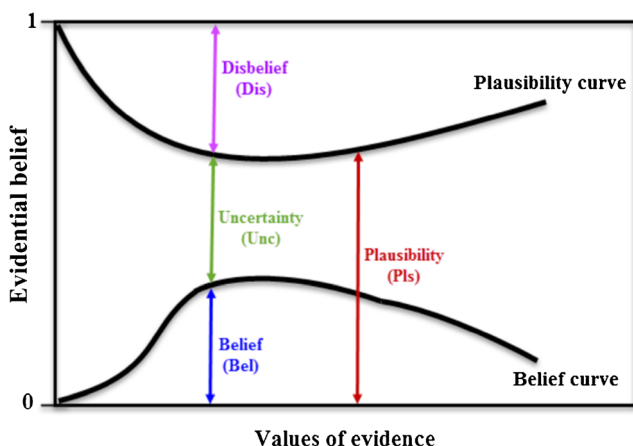


Fig. 3 Schematic relationships of evidential belief functions (Carranza et al. 2005)

On the other hand, the disbelief function (Dis) can be calculated according to Eqs. (11) and (12) (Pourghasemi and Beheshtirad 2014):

$$\left[ \lambda(\overline{T}_P)_{A_{ij}} \right] = \left[ \frac{N(W) - N(W \cap A_{ij})}{N(W)} \right] / \left[ \frac{N(P) - N(W) - N(A_{ij}) + N(W \cap A_{ij})}{N(P) - N(W)} \right] \quad (12)$$

$$(\text{Dis}) = \left[ \lambda(\overline{T}_P)_{A_{ij}} \right] / \sum \left[ \lambda(\overline{T}_P)_{A_{ij}} \right] \quad (13)$$

Uncertainty (Unc) and plausibility (Pls) functions can be determined as follows (Eqs. 13 and 14):

$$(\text{Unc}) = [1 - (\text{Bel}) - (\text{Dis})] \quad (14)$$

$$(\text{Pls}) = [1 - (\text{Dis})] \quad (15)$$

Finally, the groundwater potential map (GPM) using EBF model was produced using the following equation:

$$\begin{aligned} \text{GPM} = & [\text{Lithology}_{\text{Bel}}] + [\text{Landuse}_{\text{Bel}}] + [\text{Distance from river}_{\text{Bel}}] \\ & + [\text{Soil texture}_{\text{Bel}}] + [\text{Drainage density}_{\text{Bel}}] \\ & + [\text{Altitude}_{\text{Bel}}] + [\text{Curvature}_{\text{Bel}}] + [\text{TWI}_{\text{Bel}}] \\ & + [\text{Slope percent}_{\text{Bel}}] \end{aligned} \quad (16)$$

### Comparison and validation of the groundwater potential maps

According to Chung and Fabbri (2003), model validation is considered as the most important process of modeling. From scientific significance viewpoint, it is very essential to evaluate the resultant GPM accuracy. The receiver operating characteristics (ROC) curve was used to calculate the accuracy of the GPMs (Frattini et al. 2010; Naghibi et al. 2014; Rahmati et al. 2014a). The GPMs were verified using the groundwater well locations in the validation datasets.

According to Pourtaghi and Pourghasemi (2014), the ROC curves were plotted by considering cumulative percentage of potential maps (on the X axis) and the cumulative percentage of groundwater occurrence (on the Y axis). According to Yesilnacar (2005), the quantitative–qualitative relationship between the prediction accuracy and AUC value can be classified as follows: poor (0.5–0.6), average (0.6–0.7), good (0.7–0.8), very good (0.8–0.9), and excellent (0.9–1).



**Table 2** Spatial relationship between each conditioning factor and well locations using WOE and EBF models

Factor	Class	No. pixels in domain	No. of Wells	WOE		EBF								
				$W^+$	$W^-$	C	$S^2(W^+)$	$S^2(W^-)$	S(C)	$\tau$	Bel	Dis	Unc	Pis
Lithology	$Q_h$	220,484	97	0.089	-1.123	1.212	0.01	0.25	0.51	2.37	0.355	0.134	0.51	0.866
	PbK	29,128	3	-1.362	0.093	-1.456	0.333	0.01	0.586	-2.48	0.083	0.454	0.463	0.546
	Bk	1439	1	0.546	-0.004	0.551	1	0.01	1.005	0.54	0.561	0.412	0.027	0.588
Land use	Agriculture	146,297	87	0.39	-1.102	1.493	0.011	0.071	0.287	5.18	0.449	0.089	0.461	0.911
	Range	79,493	10	-1.162	0.276	-1.439	0.1	0.01	0.333	-4.32	0.095	0.355	0.55	0.645
	Urban	5440	3	0.315	-0.008	0.323	0.333	0.01	0.586	0.55	0.417	0.267	0.316	0.733
Distance from river (m)	Forest	19,821	1	-2.076	0.072	-2.148	1	0.01	1.005	-2.13	0.038	0.289	0.673	0.711
	<438.4	132,128	53	-0.002	0.003	-0.006	0.018	0.02	0.199	-0.03	0.258	0.202	0.54	0.798
	438.4–1048.5	75,054	37	0.203	-0.101	0.304	0.027	0.015	0.206	1.47	0.317	0.182	0.501	0.818
Soil texture	1048.5–1906.4	24,710	9	-0.099	0.01	-0.109	0.111	0.01	0.349	-0.31	0.234	0.203	0.563	0.797
	1906.4–3164.7	14,765	1	-1.782	0.05	-1.832	1	0.01	1.005	-1.82	0.044	0.211	0.745	0.789
	>3164.7	4394	1	-0.569	0.007	-0.577	1	0.01	1.005	-0.57	0.146	0.202	0.651	0.798
Drainage density (km/km <sup>2</sup> )	Clay	3828	0	0	0.015	-0.015	0	0.009	0.099	-0.15	0	0.265	0.735	0.735
	Clay loam	102,577	6	-1.928	0.464	-2.392	0.166	0.01	0.42	-5.68	0.068	0.415	0.518	0.585
	Sandy clay loam	117,877	95	0.695	-2.189	2.884	0.01	0.166	0.42	6.85	0.932	0.029	0.038	0.971
Altitude (m)	Sandy Loam	26,769	0	0	0.112	-0.112	0	0.009	0.099	-1.13	0	0.292	0.708	0.708
	<0.31	64,187	18	-0.361	0.099	-0.46	0.055	0.012	0.26	-1.76	0.155	0.274	0.57	0.726
	0.31–0.81	91,869	36	-0.026	0.014	-0.041	0.027	0.015	0.207	-0.19	0.217	0.252	0.531	0.748
Curvature	0.81–1022	66,877	26	-0.034	0.012	-0.046	0.038	0.013	0.227	-0.2	0.215	0.252	0.533	0.748
	1.22–2.16	28,118	21	0.618	-0.114	0.733	0.047	0.012	0.245	2.98	0.413	0.222	0.365	0.778
	<138	32,427	12	-0.083	0.011	-0.095	0.083	0.011	0.307	-0.31	0.202	0.204	0.594	0.796
TWI	138–163	64,862	41	0.452	-0.221	0.674	0.024	0.016	0.202	3.32	0.345	0.161	0.494	0.839
	163–188	63,600	28	0.09	-0.032	0.122	0.035	0.013	0.222	0.55	0.24	0.195	0.565	0.805
	188–217	52,536	19	-0.106	0.026	-0.132	0.052	0.012	0.254	-0.52	0.198	0.206	0.596	0.794
Slope percent	217–271	37,626	1	-2.717	0.152	-2.87	1	0.01	1.005	-2.85	0.015	0.234	0.751	0.766
	Concave	94,653	16	-0.867	0.3	-1.168	0.062	0.011	0.272	-4.28	0.138	0.453	0.409	0.547
	Flat	108,940	62	0.347	-0.382	0.729	0.016	0.025	0.204	3.56	0.465	0.228	0.306	0.772
Slope percent	Convex	47,458	23	0.186	-0.048	0.235	0.043	0.012	0.237	0.99	0.396	0.319	0.285	0.681
	<6	62,778	28	0.103	-0.036	0.14	0.035	0.013	0.222	0.63	0.277	0.241	0.482	0.759
	6–6.82	62,770	28	0.103	-0.036	0.14	0.035	0.013	0.222	0.63	0.277	0.241	0.482	0.759
Slope percent	6.82–8.09	62,768	25	-0.01	0.003	-0.013	0.04	0.013	0.23	-0.05	0.248	0.251	0.502	0.749
	>8.09	62,735	20	-0.232	0.066	-0.29	0.05	0.012	0.249	-1.19	0.198	0.267	0.535	0.733
	0–2	80,637	42	0.258	-0.15	0.408	0.023	0.016	0.201	2.02	0.309	0.171	0.52	0.829
Slope percent	2–5	114,037	36	-0.242	0.164	-0.407	0.027	0.015	0.207	-1.96	0.187	0.234	0.579	0.766

**Table 2** (continued)

Factor	Class	No. pixels in domain	No. of Wells	WOE		EBF								
				W <sup>+</sup>	W <sup>-</sup>	C	S <sup>2</sup> (W <sup>+</sup> )	S <sup>2</sup> (W <sup>-</sup> )	S (C)	τ	Bel	Dis	Unc	Pls
	5–10	46,789	19	0.009	-0.002	0.011	0.052	0.012	0.254	0.04	0.241	0.198	0.561	0.802
	10–20	8998	4	0.099	-0.003	0.103	0.25	0.01	0.51	0.2	0.263	0.198	0.539	0.802
	>20	590	0	0	0.002	-0.002	0	0.009	0.099	-0.02	0	0.199	0.801	0.801
Lineament density (km/km <sup>2</sup> )	0–0.47	190,359	60	-0.244	0.518	-0.762	0.016	0.024	0.202	-3.76	0.051	0.305	0.64	0.70
	0.47–0.94	40,126	18	0.108	-0.022	0.131	0.055	0.012	0.260	0.50	0.073	0.178	0.75	0.82
	0.94–1.41	15,126	12	0.679	-0.064	0.743	0.083	0.011	0.307	2.41	0.130	0.170	0.70	0.83
Rainfall (mm)	1.41–1.88	3723	6	1.388	-0.046	1.435	0.166	0.010	0.421	3.40	0.264	0.173	0.56	0.83
	>1.88	1717	5	1.981	-0.043	2.025	0.200	0.010	0.459	4.41	0.479	0.174	0.35	0.83
	300–310	33,534	17	0.231	-0.040	0.272	0.058	0.011	0.266	1.02	0.466	0.344	0.19	0.66
	310–320	159,966	79	0.205	-0.510	0.71	0.012	0.045	0.241	2.96	0.454	0.215	0.33	0.79
	320–330	57,552	5	-1.53	0.209	-1.74	0.20	0.010	0.458	-3.79	0.079	0.441	0.48	0.56

*Bel* belief, *Dis* disbelief, *Unc* uncertainty, *Pls* plausibility

**Sensitivity analysis**

In the current study, a map-removal sensitivity analysis was conducted for the EBF model to examine the effects of removing any of the conditioning factors on the GPMs (Fenta et al. 2015). The relative decrease (RD) of AUC values as a percentage was calculated to examining the model output with and without each factor (i.e., related to dependency of GPMs on the influence of groundwater conditioning factors) using the following equation (Eq. 15) (Oh et al. 2011; Park et al. 2014):

$$RD_i = \frac{(AUC_{all} - AUC_i)}{AUC_i} \times 100 \tag{16}$$

where AUC<sub>all</sub> indicates the AUC value obtained from the groundwater potential mapping using all conditioning factors and AUC<sub>i</sub> is the prediction accuracy when the *i*th conditioning factor has been excluded.

**Results and discussion**

**Application of WOE model for groundwater potential mapping**

In the current study, all parameters of WOE model were calculated for each groundwater conditioning factors (Table 2). Table 2 shows relevant factor’s weight (τ) and the spatial relationship between classes of each conditioning factor and the groundwater occurrence. The contrast value for the WOE model is positive and negative for a positive and negative spatial association, respectively (Lee and Choi 2004).

The analysis of WOE for the relationship between well locations and lithology units indicate that high level pediment fan and valley terrace deposits class (*Q<sub>ft</sub>*) has the highest τ value (2.37) followed by conglomerate marly and sandy conglomerate with calcareous and clay matrix (Bk) class (0.54). Quaternary deposits which are very permeable and cover a significant part of the study area are also positively correlated with groundwater occurrence. On the other hand, conglomerate locally with sandstone (Plbk) class is not positively correlated with groundwater occurrence (τ=-2.48). The compacted conglomerate rocks locally with sandstone are assumed as relatively poor groundwater potential because of difficulty in terms of groundwater storage and movement. Among the different landuse types, agriculture category had the highest τ values, showing maximum groundwater probability. This may be due to the back infiltration of irrigation water to the groundwater system which it can increase the aquifer recharge. This finding is consistent with Kumar et al. (2007) who demonstrated that landuse factor controls the infiltration and runoff process and subsequently affects

evapotranspiration and recharge of the groundwater resource. In particular, Nampak et al. (2014) stated that cropland is an excellent site form groundwater potentiality point of view. The distance from the river from 438.4 to 1048.5 m indicated positive influence in groundwater occurrence, while the areas more than 1048.5 m represented the negative correlation. In soil texture type, the highest weight of 6.85 was achieved for the sandy clay loam texture. The drainage density 1.22–2.16 km/km<sup>2</sup> has the highest final weight ( $\tau=2.98$ ), which means that the attributes of this class have the strongest relationship with groundwater occurrence. The drainage density result matches with the findings of Nampak et al. (2014) that included drainage density factor in the groundwater potential analysis for the Langat River catchment, Malaysia. Razandi et al. (2015) demonstrate that low drainage density of a given plain is indicative of low groundwater recharge. In the case of altitude, the highest weight (3.32) was for the range of 138–163 m that has a positive effect in groundwater probability. However, groundwater potential decreased in the highest areas with few deposits (i.e., related to percolation and storage processes). The analysis of WOE for the relationship between well locations and curvature layer indicated that flat area had positive influences in groundwater occurrence. Also,  $\tau$  values decreases by increasing of TWI. The previous study by Razandi et al. (2015) confirmed that there is a negative correlation between TWI and groundwater occurrence which shows a higher groundwater potential over a decreasing the TWI value. Analysis of the WOE results shows that the  $\tau$  is

2.02 for slope percent class of 2–5, indicating a high probability of groundwater occurrence within this slope percent range. This finding is in agreement with the result obtained in different studies of groundwater potential mapping (Adiat et al. 2012; Manap et al. 2014; Nampak et al. 2014). Chowdhury et al. (2009) explained that gentle slope areas facilitate infiltration and consequently promote groundwater recharge. In the case of lineament density, the classes of 0–0.47, 0.47–0.94, 0.94–1.41, 1.41–1.88, and >1.88 km/km<sup>2</sup> have weights ( $\tau$ ) of –3.76, 0.5, 2.41, 3.40, and 4.41, respectively. This indicates that the groundwater potential increases with the increase in lineament density. Chowdhury et al. (2010) stated that the lineaments often act as good conduits for groundwater recharge especially when them coupled with relatively permeable stream beds (i.e., crossing of the streams and lineaments). Rainfall has been applied because it is supposed that this variable influences the amount of water that would be available to soak/percolate into the underground. The rainfall class 310–320 mm has the highest value of  $\tau$  (2.96) followed by 300–310 mm class (1.02). The lowest value of  $\tau$  (–3.79) is for rainfall class 320–330 mm. From this, it is clear that the groundwater potential increases by the increase in rainfall, and then, it decreases because of other geo-environmental factors. According to Adiat et al. (2012), even if the study area is characterized by almost uniform annual rainfall distribution, this factor plays an important role in groundwater potential mapping. Finally, based on Eq. 8, the final GPM produced by the WOE model is shown in Fig. 4.

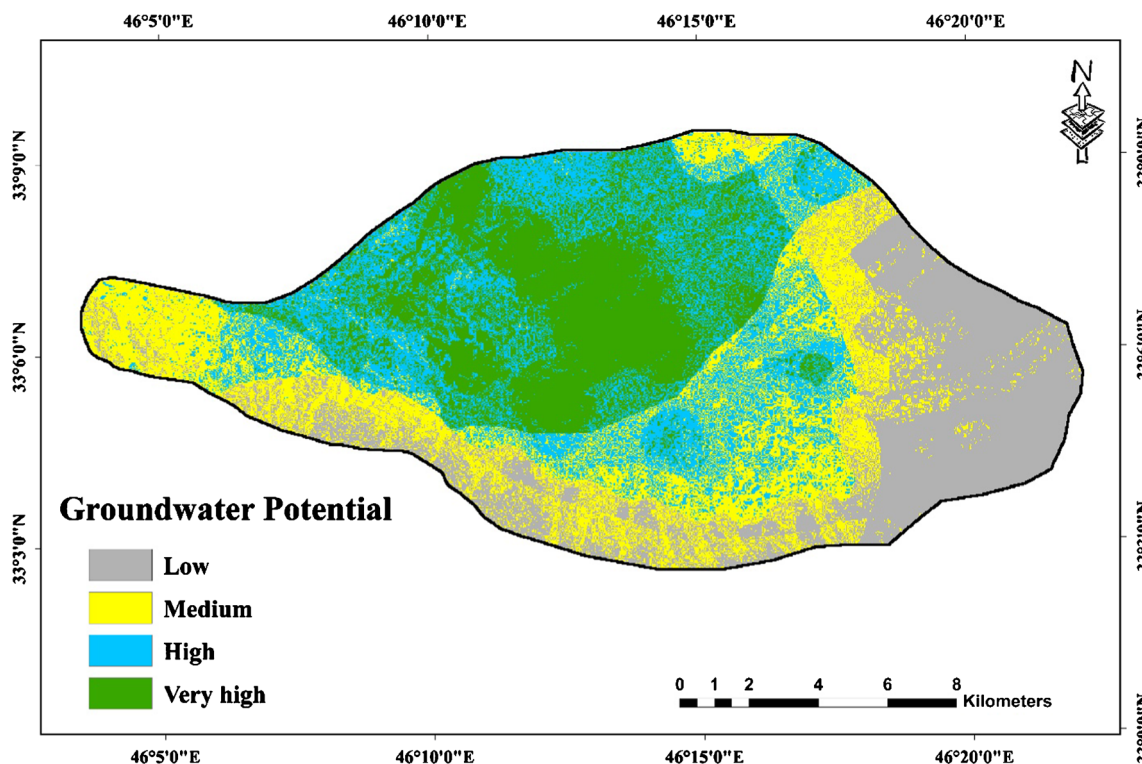


Fig. 4 Groundwater potential map based on WOE model

In the GPM, the highly groundwater potential zones are found in the central and northwest parts of the study area, where the landuse and soil texture types mainly are agriculture and sandy clay loam, respectively. Areas with high lineament density fall under high groundwater potential zone, where this finding is agree with Nampak et al. (2014). Figure 4 illustrates that the northern and western portions and some small patches in the eastern of study area are generally medium potential class. The eastern part and a few patches in the study area are dominated by low groundwater potential zone in which these areas are attributed to combinations of landuse (forest and range lands), lithology (Plbk), lineament features (low lineament density), soil texture (clay loam), and slope (moderate to steep slope).

### Application of EBF model for groundwater potential mapping

To produce GPM and determine the level of correlation between groundwater well locations and conditioning factors, the EBF model was applied. Table 2 indicates the belief

(Bel), disbelief (Dis), uncertainty (Unc), and plausibility (Pls) that was calculated for each class of each conditioning factor. A comparatively high Bel value indicates a higher probability of groundwater occurrence, while a low Bel value implies a lower probability of groundwater occurrence.

As shown in Table 2, lithology has a specific impact on the hydrogeologic condition of the study area. In details, Bk class has the highest Bel value (0.561) followed by  $Q_{ft}$  class (0.351); thus, these lithological units have the most groundwater probability. In the case of landuse, it can be seen that the agriculture and urban landuse types have belief values of 0.449 and 0.417, respectively, showing that the groundwater probability in these landuse types is very high. As stated in previous section, the agriculture landuse type is assumed as good groundwater potential due to back infiltration into groundwater system. For distance from rivers, it can be seen that as the distance from the river increases, the groundwater occurrence generally decreases. The distance range of 438.4–1048.5 m (0.317) has the highest Bel value, followed by <438.4 m (0.258). In the case of soil texture, sandy clay loam class has the highest Bel value (0.932); thus, this soil texture

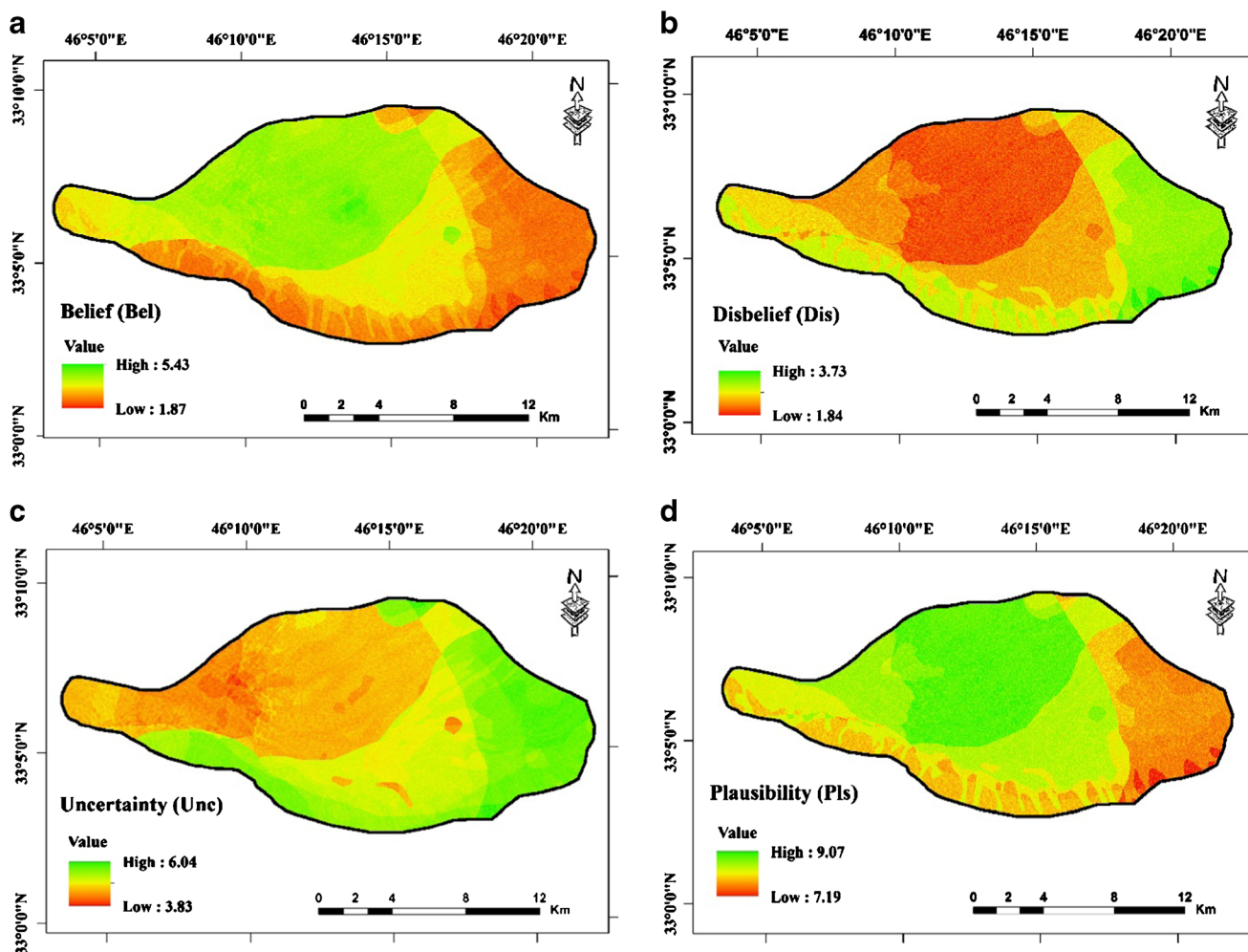


Fig. 5 Integrated results of EBF model. a Belief. b Disbelief. c Uncertainty. d Plausibility

type has the most groundwater probability in study area. In the case of drainage density, the results represented the positive relationship with degree of Bel between the denser drainage and the higher groundwater probability. The Bel value analysis indicated the highest value belonged to the drainage density of 1.22–2.16 km/km<sup>2</sup>. This result is in line with the results of Nampak et al. (2014) that applied drainage density layer in the EBF model to groundwater potential mapping for the Langat River catchment, Malaysia. Furthermore, assessment of altitude showed that the class of 138–163 m has the highest Bel value (0.345). According to study of Manap et al. (2013) as the altitude increased, the groundwater occurrence generally decreased, since topographic conditions of the areas with low altitude are not suitable for groundwater recharge and storage. For curvature, the highest Bel value belongs to the classes of flat (0.465) and convex (0.396), while the lowest Bel values are observed for the concave class (0.138). In the case of TWI, it can be seen that as the TWI increased, the groundwater occurrence generally decreased. For TWI less than 6.86, the Bel value, indicated a high groundwater probability. A similar trend was also reported by Razandi et al. (2015). The analysis of EBF for the relationship between groundwater well and slope percent indicate that slope percent class 0–2 has the highest value of Bel (0.309) followed by 10–20 class (0.263). This result reflects the inverse relationship

of slope percent with groundwater occurrence. Nampak et al. (2014) stated that as the slope percent decreases, the infiltration rate increases and consequently percolation and groundwater recharge increases. According to Adiat et al. (2012) and Kumar et al. (2014) in the gentle slope area, the overland flow is slow allowing more time for rainwater to soak into subsurface (i.e., infiltration process), whereas steep slope area promote the runoff generation (i.e., less residence time for infiltration of rainwater).

For the lineament density, groundwater potential is highest at the lineament density of >1.88 km/km<sup>2</sup> followed by 1.41–1.88 km/km<sup>2</sup>. Meanwhile, lineament density 0.94–1.41, 0.47–0.94, and 0–0.47 km/km<sup>2</sup> show low Bel value, 0.13, 0.073 and 0.051, respectively. These findings agree with Lee et al. (2012a, 2012b, 2012c). Kumar et al. (2014), and Fenta et al. (2015), which indicated that high lineament density areas are favorable for groundwater potential because they facilitate percolation process and consequently promote groundwater recharge. In the case of rainfall, it is seen that the groundwater potential increases from 300 to 310 mm, and it gradually decreases from 310 mm upward. This may be due to the decrease in infiltration rate of impermeable surfaces in the upland area, as well as due to geomorphological and topographical attributes which contribute high runoff (Pradhan 2009).

The EBF results are shown in Fig. 5. The belief map (Fig. 5a) was compared to the disbelief map (Fig. 5b) which

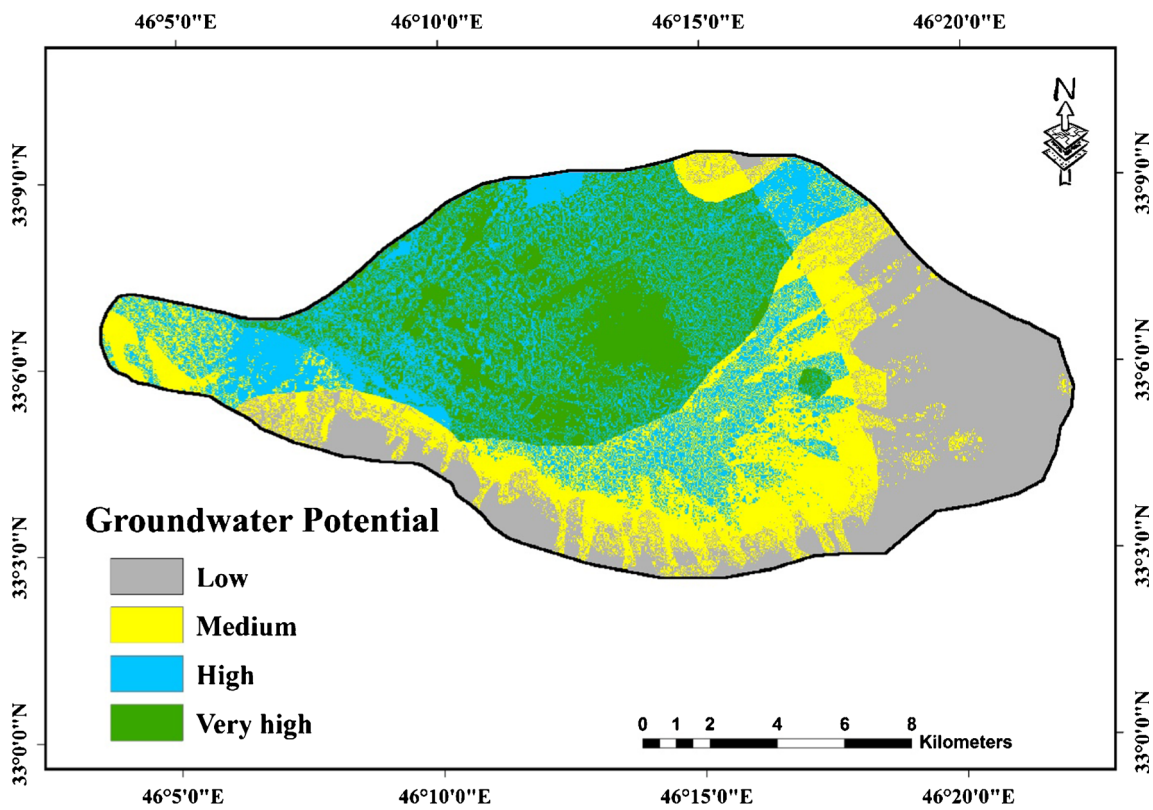


Fig. 6 Groundwater potential map based on EBF model

indicated that Bel values were low for areas where Dis values are high and vice versa. Analysis of these maps demonstrates that high groundwater probability is for the areas where there is high degree of Bel and low degree of Dis for the groundwater well occurrence. The uncertainty map (Fig. 5c) indicates lack of information to provide a real prove for groundwater occurrences. According to EBF analysis, the high uncertainty values are belonging to the areas where belief values are low.

Moreover, the plausibility map (Fig. 5d) shows high values for the areas where uncertainty value relatively is low.

The GPM was conducted based on the belief function and was classified into four classes using quantile classification scheme (Tehrany et al. 2014) as presented in Fig. 6. The “high” and “very high” groundwater potential zones mainly encompass agriculture areas with sandy clay loam soil texture around the lineament systems (i.e., high lineament density

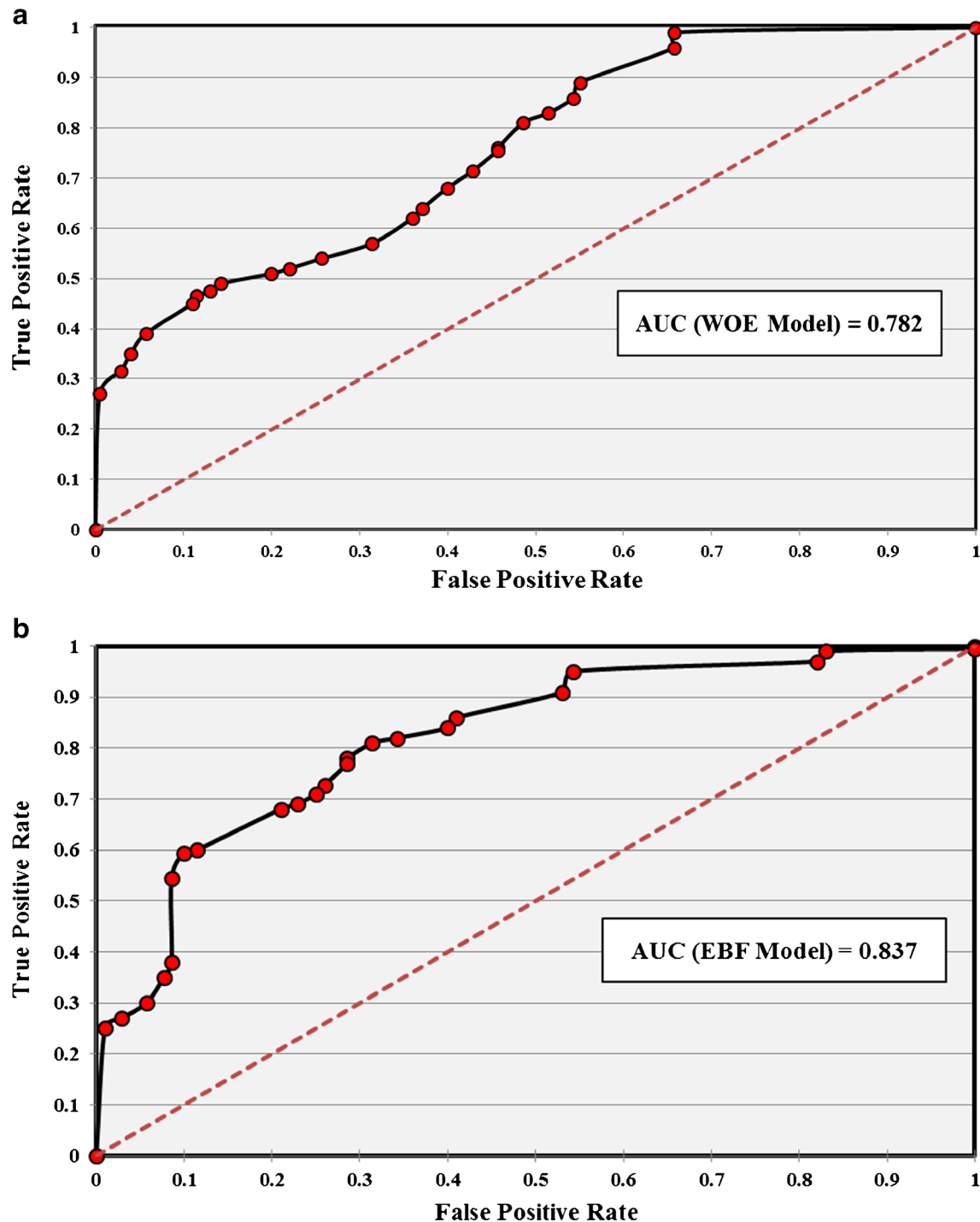


Fig. 7 ROC curves for the groundwater potential maps produced by a WOE and b EBF models

areas). The northwest and central portions of the study area fall under these zones. The south portion and some small patches in the northeast, northwest central, and west portions of the study area almost fall under “medium” groundwater potential zone. Moreover, the eastern parts and some small sites in the southern of the study area because of high slope, high altitude, low lineament density, and lithology with low permeability as well as the existence of rock-outcrops cover fall under low groundwater potential zones.

### Validation of the groundwater potential maps

The final step is to validate the constructed maps and compare the predictive performance of the WOE model with the EBF model. Therefore, the validation was conducted using the receiver operating characteristic (ROC) curve and the area under curve (AUC) was prepared (Davoodi Moghaddam et al. 2015; Pourtaghi and Pourghasemi 2014). In the ROC curve, the sensitivity of the groundwater potential model is plotted against 1-specificity (Mohammady et al. 2012; Regmi et al. 2014; Rahmati et al. 2015). Figure 7a, b indicates the ROC curve of the GPMs obtained using WOE and EBF models. These ROC curves indicate that the EBF model (AUC=83.7 %) performs better than WOE model (AUC=78.2 %). Therefore, it can be seen that the EBF and WOE models applied in the current study indicated reasonably good accuracy in spatial predicting the groundwater potentiality. As it can be seen in the current study, the groundwater potential map can be produced using WOE and EBF models which are easily performable and hence are widely can be utilized, especially in developing and low-income countries. These findings agree with Mogaji et al. (2014). Nampak et al. (2014), and Park et al. (2014), which indicated that EBF can be used as an efficient bivariate model in groundwater potential mapping. In addition, according to Corsini et al. (2009). WOE showed good estimator for groundwater potential mapping.

### Sensitivity analysis of the groundwater potential map

The result of the sensitivity analysis—for the EBF model—as a decrease of AUC values (i.e., loss of performance) is summarized in Table 3. The most influential factors were land use (RD=3.563 %), soil texture (RD=about 3.2 %), lineament density (RD=about 3 %), and TWI (RD=about 2 %), which afforded the largest decrease of AUC values when excluded in the groundwater potential modeling. The GPM is moderately sensitive to rainfall, slope percent, altitude, distance from river, and drainage density with RD of 1.344, 1.166, 0.89, 0.611, and 0.585 %, respectively; however, it is less sensitive to lithology (RD=0.115 %) and curvature (RD=0.074 %). In this study, lithology was not so important factor since  $Q_f$  class occupies most of the study area. However, it is widely acknowledged that the importance of variables in groundwater

**Table 3** Sensitivity analysis results in terms of the relative decrease (RD) of AUC values when each groundwater conditioning factor is excluded in the EBF model

Excerpted factor	Relative decrease (RD) of AUC (%)
Lithology	0.115
Land use	3.563
Distance from river	0.611
Soil texture	3.197
Drainage density	0.585
Altitude	0.890
Curvature	0.074
TWI	1.982
Slope percent	1.166
Lineament density	3.040
Rainfall	1.344

potential mapping is noticeably affected by properties of study area and method used in a research (Naghbi and Pourghasemi 2015).

### Conclusion

The study assesses the application of GIS-based WOE and EBF models and remote sensing techniques as spatial prediction tools for groundwater potential mapping. In order to achieve the set objectives, a total of 11 geo-environmental factors (i.e., lithology, land use, distance from river, soil texture, drainage density, altitude, curvature, TWI, slope percent, lineament density, rainfall) believed to be influencing groundwater potential in the area were selected. The Ilam Plain, Iran, was selected as the study area for assessing groundwater potential zones. As a first step, using database of Iranian Department of Water Resources Management (IDWRM 2013) and extensive field surveys a well inventory map was created. The groundwater conditioning factors were then integrated in a geo-spatial database using WOE and EBF models, which analyzed the relationship between groundwater yield values and the geo-environmental factors. Finally, for testing the accuracy of the both models, the ROC curves were prepared. The produced groundwater potential maps using WOE and EBF models were validated to give 75.66 and 79.43 % accuracy, respectively. In addition, based on the results of sensitivity analyses, the GPM of study area is most sensitive to land use, soil texture, lineament density, and TWI with a relative decrease (RD) of AUC of about 3.5, 3.2, 3, and 2 %, respectively.

It has been established in the study that GIS-based WOE and EBF models are capable of producing accurate and reliable prediction. These models have provided a quick and

comprehensive prediction of groundwater potential map and also the efficiency of the predicted potential map has been quantified for applying in any other studies particularly for groundwater potential assessment. The advantage of EBF model is that it can manage uncertainties in multi resources spatial data integration and allows analysis both systemic and stochastic uncertainty. The advantage of using WOE model rather than EBF model is its simplicity (i.e., both the model implementation and interpretation of the results). However, the WOE and EBF models have three major disadvantages: (1) because the weight value is dependent on the number of groundwater well pixels used on the groundwater potential mapping, the models underestimates or overestimates weight values if the area of a factor class is very small and the groundwater wells are not evenly distributed. (2) The weight values computed for different areas are not comparable in terms of the degree of groundwater potentiality. (3) The spatial data always have not independence condition.

The result of groundwater potential map is useful for planners in the groundwater resource management and comprehensive investigation of groundwater exploration development for future planning. For consequent research work, the use of EBF model as a cost and time effective means is suggested for managing uncertainty associated in groundwater potential mapping in the field of hydrogeological study.

**Acknowledgments** We are grateful to anonymous referees for useful insights which improved a previous version of this manuscript. Also, we thank to Iranian Department of Water Resources Management (IDWRM) and department of Geological Survey of Iran (GSI) for providing necessary data and maps.

## References

- [IDWRM] Iranian Department of Water Resources Management (2013) Weather and climate report, Tehran province. <http://www.thrw.ir/>. Accessed 25 June 2013
- Adiat KAN, Nawawi MNM, Abdullah K (2012) Assessing the accuracy of GIS-based elementary multi criteria decision analysis as a spatial prediction tool—a case of predicting potential zones of sustainable groundwater resources. *J Hydrol* 440:75–89
- Adji TN, Sejati SP (2014) Identification of groundwater potential zones within an area with various geomorphological units by using several field parameters and a GIS approach in Kulon Progo Regency, Java, Indonesia. *Arab J Geosci* 7:161–172
- Al Saud M (2010) Mapping potential areas for groundwater storage in Wadi Aurnah Basin, western Arabian Peninsula, using remote sensing and geographic information system techniques. *Hydrogeol J* 18: 1481–1495
- Alavi M (1994) Tectonics of the Zagros orogenic belt of Iran; new data and interpretations. *Tectonophysics* 229:211–238
- Althuwaynee OF, Pradhan B, Lee S (2012) Application of an evidential belief function model in landslide susceptibility mapping. *Comput Geosci* 44:120–135
- Althuwaynee OF, Pradhan B, Park HJ, Lee JH (2014) A novel ensemble bivariate statistical evidential belief function with knowledge-based analytical hierarchy process and multivariate statistical logistic regression for landslide susceptibility mapping. *Catena* 114:21–36
- Awawdeh M, Obeidat M, Al-Mohammad M, Al-Qudah K, Jaradat R (2013) Integrated GIS and remote sensing for mapping groundwater potentiality in the Tulul al Ashaqif, Northeast Jordan. *Arab J Geosci*. doi:10.1007/s12517-013-0964-8
- Banks D, Robins N (2002) An introduction to groundwater in crystalline bedrock. *Norges geologiske undersøkelse, Trondheim*, p 64
- Bevan MJ, Endres AL, Rudolph DL, Parkin G (2005) A field scale study of pumping-induced drainage and recovery in an unconfined aquifer. *J Hydrol* 315:52–70
- Bonham-Carter GF (1991) Integration of geoscientific data using GIS. In: Goodchild MF, Rhind DW, Maguire DJ (eds) *Geographic information systems: principle and applications*. Longdom, London, pp 171–184
- Bonham-Carter GF (1994) Geographic information systems for geoscientists: modeling with GIS. In: Bonham-Carter F (ed) *Computer methods in the geosciences*. Pergamon, Oxford
- Carranza EJM (2009) Controls on mineral deposit occurrence inferred from analysis of their spatial pattern and spatial association with geological features. *Ore Geol Rev* 35:383–400
- Carranza EJM, Hale M (2003) Evidential belief functions for data-driven geologically constrained mapping of gold potential, Baguio district, Philippines. *Ore Geol Rev* 22:117–132
- Carranza E, Woldai T, Chikambwe E (2005) Application of data-driven evidential belief functions to prospectivity mapping for aquamarine-bearing pegmatites, Lundazi district, Zambia. *Nat Resour Res* 14: 47–63
- Carranza EJM, Van Ruitenbeek F, Hecker C, van der Meijde M, van der Meer FD (2008) Knowledge-guided data-driven evidential belief modeling of mineral prospectivity in Cabo de Gata, SE Spain. *Int J Appl Earth Obs* 10:374–387
- Chang TC, Chien YH (2007) The application of genetic algorithm in debris flows prediction. *Environ Geol* 53:339–347
- Chen J, Zhang Y, Chen Z, Nie Z (2014) Improving assessment of groundwater sustainability with analytic hierarchy process and information entropy method: a case study of the Hohhot Plain. *China Environ Earth Sci*. doi:10.1007/s12665-014-3583-0
- Chenini I, Mammou AB (2010) Groundwater recharge study in arid region: an approach using GIS techniques and numerical modelling. *Comput Geosci* 36(6):801–817
- Chenini I, Mammou AB, May MY (2010) Groundwater recharge zone mapping using GIS-based multi-criteria analysis: a case study in Central Tunisia (Maknassy Basin). *Water Resour Manag* 24:921–939
- Chowdhury A, Jha MK, Chowdary VM, Mal BC (2009) Integrated remote sensing and GIS-based approach for assessing groundwater potential in West Medinipur district, West Bengal, India. *Int J Remote Sens* 30(1):231–250
- Chowdhury A, Jha MK, Chowdary VM (2010) Delineation of groundwater recharge zones and identification of artificial recharge sites in West Medinipur District, West Bengal using RS, GIS and MCDM techniques. *Environ Earth Sci* 59(6):1209–1222
- Chung JF, Fabbri AG (2003) Validation of spatial prediction models for landslide hazard mapping. *Nat Hazards* 30(3):451–472
- Corsini A, Cervi F, Ronchetti F (2009) Weight of evidence and artificial neural networks for potential groundwater spring mapping: an application to the Mt. Modino area (Northern Apennines, Italy). *Geomorphology* 111:79–87
- Dar IA, Sankar K, Dar MA (2010) Remote sensing technology and geographic information system modeling: an integrated approach towards the mapping of groundwater potential zones in Hardrock terrain, Mamundiyar basin. *J Hydrol* 394:285–295
- Davoodi Moghaddam D, Rezaei M, Pourghasemi HR, Pourtaghie ZS, Pradhan B (2015) Groundwater spring potential mapping using



- bivariate statistical model and GIS in the Taleghan watershed, Iran. Arab J Geosci 8(2):913–929
- Dempster AP (1968) A generalization of bayesian inference. J Roy Stat Soc 30:205–247
- Elewa HH, Qaddah AA (2011) Groundwater potentiality mapping in the Sinai Peninsula, Egypt, using remote sensing and GIS-watershed based modeling. Hydrogeol J 19:613–628
- Elmahdy SI, Mostafa Mohamed M (2014) Groundwater potential modelling using remote sensing and GIS: a case study of the Al Dhaid area, United Arab Emirates. Geocarto Int 29(4):433–450
- Ettazarini S (2007) Groundwater potential index: a strategically conceived tool for water research in fractured aquifers. Environ Geol 52:477–487
- Ettazarizini S, El Mahmoudi N (2004) Vulnerability mapping of the Turonian limestone aquifer in the phosphate plateau (Morocco). Environ Geol 46:113–117
- Fashae OA, Tijani MN, Talabi AO, Adedeji OI (2014) Delineation of groundwater potential zones in the crystalline basement terrain of SW-Nigeria: an integrated GIS and remote sensing approach. Appl Water Sci 4:19–38
- Fenta AA, Kifle A, Gebreyohannes T, Hailu G (2015) Spatial analysis of groundwater potential using remote sensing and GIS-based multi-criteria evaluation in Raya Valley, northern Ethiopia. Hydrogeol J 23:195–206
- Fratini P, Crosta G, Carrara A (2010) Techniques for evaluating the performance of landslide susceptibility models. Eng Geol 111:62–72
- Ganapuram S, Kumar GTV, Krishna IVM, Kahya E, Demirel MC (2009) Mapping of groundwater potential zones in the Musi basin using remote sensing data and GIS. Adv Eng Softw 40:506–518
- Geology Survey of Iran (GSI) (1997) [http://www.gsi.ir/Main/Lang\\_en/index.html](http://www.gsi.ir/Main/Lang_en/index.html)
- Ghayoumian J, Mohseni Saravi M, Feiznia S, Nouri B, Malekian A (2007) Application of GIS techniques to determine areas most suitable for artificial groundwater recharge in a coastal aquifer in southern Iran. J Asian Earth Sci 30(2):364–374
- Gupta M, Srivastava PK (2010) Integrating GIS and remote sensing for identification of groundwater potential zones in the hilly terrain of Pavagarh, Gujarat, India. Water Int 35(2):233–245
- Hammouri N, El-Naqa A, Barakat M (2012) An integrated approach to groundwater exploration using remote sensing and geographic information system. J Water Resour Protect 4:717–724
- Israil M, Al-hadithi M, Singhal DC (2006) Application of a resistivity survey and geographical information system (GIS) analysis for hydrogeological zoning of a piedmont area, Himalayan foothill region, India. Hydrogeol J 14:753–759
- Jha MK, Chowdhury A, Chowdhury VM, Peiffer S (2007) Groundwater management and development by integrated remote sensing and geographic information systems: prospects and constraints. Water Resour Manag 21:427–467
- Jha MK, Chowdhury VM, Chowdhury A (2010) Groundwater assessment in Salboni Block, West Bengal (India) using remote sensing, geographical information system and multi-criteria decision analysis techniques. Hydrogeol J 18:1713–1728
- Kaliraj S, Chandrasekar N, Magesh NS (2014) Identification of potential groundwater recharge zones in Vaigai upper basin, Tamil Nadu, using GIS-based analytical hierarchical process (AHP) technique. Arab J Geosci 7:1385–1401
- Kumar PKD, Gopinath G, Seralathan P (2007) Application of remote sensing and GIS for demarcation of ground water potential zones of a river basin in Kerala, southwest coast of India. Int J Remote Sens 28(24):5583–5601
- Kumar T, Gautam AK, Kumar T (2014) Appraising the accuracy of GIS-based Multi-criteria decision making technique for delineation of Groundwater potential zones. Water Resour Manag 28:4449–4466
- Lee S, Choi J (2004) Landslide susceptibility mapping using GIS and the weight-of-evidence model. Int J Geogr Inf Sci 18(8):789–814
- Lee S, Hwang J, Park I (2012a) Application of data-driven evidential belief functions landslide susceptibility mapping in Jinbu, Korea. Catena 100:15–30
- Lee S, Kim YS, Oh HJ (2012b) Application of a weights-of-evidence method and GIS to regional groundwater productivity potential mapping. J Environ Manag 96(1):91–105
- Lee S, Song KY, Kim Y, Park I (2012c) Regional groundwater productivity potential mapping using a geographic information system (GIS) based artificial neural network model. Hydrogeol J 20(8):1511–1527
- Liu Y, Guo HC, Zou R, Wang J (2006) Neural network modelling for regional hazard assessment of debris flow in Lake Qionghai Watershed, China. Environ Geol 49:968–976
- Machiwal D, Jha MK, Mal BC (2011) Assessment of groundwater potential in a semi-arid region of India using remote sensing, GIS and MCDM techniques. Water Resour Manag 25:1359–1386
- Madrucci V, Taioli F, Araujo CCD (2008) Groundwater favorability map using GIS multicriteria data analysis on crystalline terrain, Sao Paulo State, Brazil. J Hydrol 357:153–173
- Magesh NS, Chandrasekar N, Soundranayagam JP (2012) Delineation of groundwater potential zones in Theni district, Tamil Nadu, using remote sensing, GIS and MIF techniques. Geosci Front 3(2):189–196
- Manap MA, Sulaiman WNA, Ramli MF, Pradhan B, Surip N (2013) A knowledge-driven GIS modeling technique for groundwater potential mapping at the Upper Langat Basin, Malaysia. Arab J Geosci 6:1621–1637
- Manap MA, Nampak H, Pradhan B, Lee S, Sulaiman WNA, Ramli MF (2014) Application of probabilistic-based frequency ratio model in groundwater potential mapping using remote sensing data and GIS. Arab J Geosci 7:711–724
- Mogaji KA, Lim HS, Abdullah K (2014) Regional prediction of groundwater potential mapping in a multifaceted geology terrain using GIS-based Dempster–Shafer model. Arab J Geosci. doi:10.1007/s12517-014-1391-1
- Mohammady M, Pourghasemi HR, Pradhan B (2012) Landslide susceptibility mapping at Golestan Province, Iran: a comparison between frequency ratio, Dempster–Shafer, and weights-of-evidence models. J Asian Earth Sci 61:221–236
- Moore ID, Grayson RB, Ladson AR (1991) Digital terrain modeling: a review of hydrological, geomorphological and biological applications. Hydrol Process 5:3–30
- Nag SK, Ghosh P (2013) Delineation of groundwater potential zone in Chhatna Block, Bankura District, West Bengal, India using remote sensing and GIS techniques. Environ Earth Sci 70(5):2115–2127
- Nag SK, Saha S (2014) Integration of GIS and remote sensing in groundwater investigations: a case study in Gangajalghati Block, Bankura District, West Bengal, India. Arab J Sci Eng 39(7):5543–5553
- Nag A, Ghosh S, Biswas S, Sarkar D, Sarkar PP (2012) An image steganography technique using X-box mapping. Advances in Engineering, Science and Management (ICAESM), International Conference. pp. 709–713. IEEE
- Naghbi SA, Pourghasemi HR (2015) A comparative assessment between three machine learning models and their performance comparison by bivariate and multivariate statistical methods in groundwater potential mapping. Water Resour Manag. doi:10.1007/s11269-015-1114-8
- Naghbi SA, Pourghasemi HR, Pourtaghie ZS, Rezaei A (2014) Groundwater qanat potential mapping using frequency ratio and Shannon's entropy models in the Moghan Watershed, Iran. Earth Sci Inform. doi:10.1007/s12145-014-0145-7
- Nampak H, Pradhan B, Manap MA (2014) Application of GIS based data driven evidential belief function model to predict groundwater potential zonation. J Hydrol 513:283–300

- NRMAI [Natural Resources Management Agency of Iran] (2005) Water resources management and GIS-based landscape evolution report. Natural resources management agency of Iran, Tehran
- Oh HJ, Kim YS, Choi JK, Park E, Lee S (2011) GIS mapping of regional probabilistic groundwater potential in the area of Pohang City, Korea. *J Hydrol* 399(3):158–172
- Ozdemir A (2011) GIS-based groundwater spring potential mapping in the Sultan Mountains (Konya, Turkey) using frequency ratio, weights of evidence and logistic regression methods and their comparison. *J Hydrol* 411:290–308
- Park NW (2011) Application of Dempster–Shafer theory of evidence to GIS-based landslide susceptibility analysis. *Environ Earth Sci* 62(2):367–376
- Park I, Kim Y, Lee S (2014) Groundwater productivity potential mapping using evidential belief function. *Ground Water* 52:201–207
- Pourghasemi HR, Beheshtirad M (2014) Assessment of a data-driven evidential belief function model and GIS for groundwater potential mapping in the Koohrang Watershed, Iran. *Geocarto Int*. doi:10.1080/10106049.2014.966161
- Pourghasemi HR, Moradi HR, Fatemi Aghda SM, Gokceoglu C, Pradhan B (2013a) GIS-based landslide susceptibility mapping with probabilistic likelihood ratio and spatial multi-criteria evaluation models (North of Tehran, Iran). *Arab J Geosci*. doi:10.1007/s12517-012-0825-x
- Pourghasemi HR, Pradhan B, Gokceoglu C, Mohammadi M, Moradi HR (2013b) Application of weights-of-evidence and certainty factor models and their comparison in landslide susceptibility mapping at Haraz watershed, Iran. *Arab J Geosci* 6:2351–2365
- Pourtaghi ZS, Pourghasemi HR (2014) GIS-based groundwater spring potential assessment and mapping in the Birjand Township, southern Khorasan Province, Iran. *Hydrogeol J*. doi:10.1007/s10040-013-1089-6
- Pradhan B (2009) Groundwater potential zonation for basaltic watersheds using satellite remote sensing data and GIS techniques. *Cent Eur J Geosci* 1(1):120–129
- Pradhan B, Oh HJ, Buchroithner M (2010) Weights-of-evidence model applied to landslide susceptibility mapping in a tropical hilly area. *Geomatics Nat Hazards Risk* 1(3):199–223
- Prasad RK, Mondal NC, Banerjee P, Nandakumar MV, Singh VS (2008) Deciphering potential groundwater zone in hard rock through the application of GIS. *Environ Geol* 55(3):467–475
- Rahmati O, Nazari Samani A, Mahdavi M, Pourghasemi HR, Zeinivand H (2014a) Groundwater potential mapping at Kurdistan region of Iran using analytic hierarchy process and GIS. *Arab J Geosci*. doi:10.1007/s12517-014-1668-4
- Rahmati O, Nazari Samani A, Mahmoodi N, Mahdavi M (2014b) Assessment of the contribution of N-fertilizers to nitrate pollution of groundwater in Western Iran (case study: Ghorveh–Dehgelan Aquifer). *Water Qual Expo Health*. doi:10.1007/s12403-014-0135-5
- Rahmati O, Pourghasemi HR, Zeinivand H (2015) Flood susceptibility mapping using frequency ratio and weights-of-evidence models in the Golastan Province, Iran. *Geocarto Int*. doi:10.1080/10106049.2015.1041559
- Rahmati O, Pourghasemi HR, Melesse AM (2016) Application of GIS-based data driven random forest and maximum entropy models for groundwater potential mapping: a case study at Mehran Region, Iran. *Catena* 137:360–372
- Razandi Y, Pourghasemi HR, Samani Neisani N, Rahmati O (2015) Application of analytical hierarchy process, frequency ratio, and certainty factor models for groundwater potential mapping using GIS. *Earth Sci Inform*. doi:10.1007/s12145-015-0220-8
- Regmi AD, Devkota KC, Yoshida K, Pradhan B, Pourghasemi HR, Kumamoto T, Akgun A (2014) Application of frequency ratio, statistical index, and weights-of-evidence models and their comparison in landslide susceptibility mapping in Central Nepal Himalaya. *Arab J Geosci* 7(2):725–742
- Rekha VB, Thomas AP (2007) Integrated remote sensing and GIS for groundwater potentially mapping in Koduvan Ar-Sub-watershed of Meenachil river basin, Kottayam District, Kerala. School of environmental sciences. Mahatma Gandhi University, Kerala
- Sener E, Davraz A, Ozcelik M (2005) An integration of GIS and remote sensing in groundwater investigations: a case study in Burdur, Turkey. *Hydrogeol J* 13(5–6):826–834
- Shafer GA (1976) Mathematical theory of evidence. Princeton University Press, Princeton, NJ
- Shahid S, Nath SK, Kamal ASMM (2002) GIS integration of remote sensing and topographic data using fuzzy logic for ground water assessment in Midnapur District, India. *Geocarto Int* 17(3):69–74
- Shekhar S, Pandey AC (2014) Delineation of groundwater potential zone in hard rock terrain of India using remote sensing, geographical information system (GIS) and analytic hierarchy process (AHP) techniques. *Geocarto Int*. doi:10.1080/10106049.2014.894584
- Singh AK, Prakash SR (2002) An integrated approach of remote sensing, geophysics and GIS to evaluation of groundwater potentiality of Ojhala subwatershed, Mirzapur district, UP, India. *Asian Conference on GIS, GPS, Aerial Photography and Remote Sensing, Bangkok-Thailand*
- Tangestani MH, Moore F (2002) The use of Dempster–Shafer model and GIS in integration of geoscientific data for porphyry copper potential mapping, north of Shahr-e-Babak, Iran. *Int J Appl Earth Obs Geoinf* 4:65–74
- Tehrany MS, Pradhan B, Jebur MN (2013) Spatial prediction of flood susceptible areas using rule based decision tree (DT) and a novel ensemble bivariate and multivariate statistical models in GIS. *J Hydrol* 504:69–79
- Tehrany MS, Pradhan B, Jebur MN (2014) Flood susceptibility mapping using a novel ensemble weights-of-evidence and support vector machine models in GIS. *J Hydrol* 512:332–343
- Tien Bui D, Pradhan B, Lofman O, Revhaug I, Dick OB (2012) Spatial prediction of landslide hazards in Hoa Binh province (Vietnam): a comparative assessment of the efficacy of evidential belief functions and fuzzy logic models. *Catena* 96:28–40
- Todd DK, Mays LW (1980) *Groundwater hydrology*, 2nd edn. Wiley Canada, New York
- Todd DK, Mays LW (2005) *Groundwater hydrology*, 3rd edn. Wiley, Hoboken, NJ, p 636
- Yesilnacar EK (2005) The application of computational intelligence to landslide susceptibility mapping in Turkey. Ph.D Thesis Department of Geomatics the University of Melbourne, pp 423